Scientific Research Publishing

Open Journal of Microphysics, 2023, 13, 15-26
https://www.scirp.org/journal/ojm
ISSN Online: 2162-2469
ISSN Print: 2162-2450

An *ab Initio* Study of Mechanical and Electronic Properties of Stable Phases of $CsXBr_3$ (X = Ge, Si) Compounds for Solar Cell Applications

Kennedy Juma Wanyama[1*], Phillip Wilfsen Otieno Nyawere[1], James Sifuna[2]

[1]Department of Physical and Biological Sciences, Kabarak University, Nakuru, Kenya
[2]Department of Natural Sciences, Catholic University of Eastern Africa, Nairobi, Kenya
Email: *kennedyjuma4@gmail.com, pnyawere@gmail.com, jsifuna@gmail.com

How to cite this paper: Juma Wanyama, K., Nyawere, P.W.O. and Sifuna, J. (2023) An *ab Initio* Study of Mechanical and Electronic Properties of Stable Phases of $CsXBr_3$ (X = Ge, Si) Compounds for Solar Cell Applications. *Open Journal of Microphysics*, **13**, 15-26.
https://doi.org/10.4236/ojm.2023.132002

Received: May 13, 2023
Accepted: May 27, 2023
Published: May 30, 2023

Abstract

Utilising the density functional theory, the mechanical and electrical characteristics of Cesium Germanium Bromide, $CsGeBr_3$ and Cesium Silicon Bromide $CsSiBr_3$ compounds were computed. The complicated and unique physical and chemical properties of these materials include the ideal geometric property, a limited electronic band structure, a charge density distribution, and specific van Hove singularities in the electronic density of states. With the use of the quantum espresso code and pseudo-potentials taken from the quantum espresso data repository, we have applied density functional theory. Plane Wave (PW) basis set and Projector Augmented Wave (PAW) pseudo potentials were used to compute the ground state energy. For the exchange correlation, where plane wave basis sets are used to expand the electronic structure wave function, the Generalised Gradient Approximation (GGA) was employed. For the computation of mechanical behaviour, including the bulk modulus and elastic constants with their derivatives, Thermo_pw was used as a post-processing algorithm. The theoretical framework that is being taught gives a thorough understanding of the many qualities and possible uses for solar cells and other opto-electronic devices. Both the cubic (high-temperature) and tetragonal (low-temperature) phases of $CsGeBr_3$ were discovered to have an appropriate gap for solar cells. The edge-sharing monoclinic phase exhibits a greater distortion of the band structure than the cubic phase, which has a lower total energy and a somewhat bigger electronic gap. Although our estimations are less definite because the matching silicon-based compounds have not yet been created, they nonetheless point to a small gap for cubic $CsGeBr_3$ of about 0.2 - 0.8 eV.

Keywords

Electronic, Mechanical Stability, Perovskite

1. Introduction

Since they can supply energy that cannot be depleted and are effective at turning heat energy into electricity, solar cells have emerged as the leading energy-use systems in our daily lives. Between the layers that carry electrons and holes is an absorber layer, which is one of the unique features of the solar cell. This layer is essential because it emits electron-hole pairs while absorbing electromagnetic radiation. However, these components' mechanical, electrical, and optical characteristics are also very important. According to [1], they are crucial for defining the production of light-generated currents and providing the optimal combination of the three different kinds of core components.

Because of their superior photo-electronic properties, inorganic perovskite compounds like $CsXBr_3$ (X = Ge, Si) have garnered increased interest for energy harvesting applications. Due to its hazardous characteristics, there are several restrictions that hinder the widespread use of lead [2]. Currently, lead can be replaced in solar cells and other opto-electronic applications by the lead-free $CsXBr_3$ (X = Ge, Si) compounds.

The effective mass approximation, the tight-binding model, and first-principles calculations have all been used to theoretically examine the mechanical and electrical properties of the $CsGeBr_3$ and $CsSiBr_3$ materials. The best method for determining the ideal geometric, electrical, and mechanical properties of these compounds has been shown to be first-principles calculation [3]. Depending on the type of approximations, the gap values of $CsGeBr_3$ range from 0.82 to 7.91 eV, making it a direct band gap semiconductor material, according to theoretical predictions. According to [4] the Perdew-Burke-Ernzerh of (PBE)-sol functional gave $CsGeBr_3$ an energy band gap of 1.46 eV.

When using the hybrid functional (HSE) approximation, the energy gap accuracy may be increased with the typical values of 2.34 eV for $CsGeBr_3$. Because these electron-hole bound states have a significant impact on the charge separations, the generation of excitons is necessary for a solar cell to function. Although effective mass models have provided qualitative estimates of the exciton effects in a wide range of materials, including $CsGeBr_3$, the quantitative investigation of these bound states is somewhat constrained.

Analysing some of the main characteristics of compounds, such as ductility and brittleness, requires a thorough understanding of their mechanical properties in the solid form. The elastic constants are used in solid-state physics to anticipate the mechanical characteristics of compounds and to make inferences about the relationships between mechanical characteristics and the types of forces that occur in solids. The three independent elastic constants in a cubic crystal are C_{11}, C_{12}, and C_{44}. The total energies of a stretched crystal are fixed to a fourth-order polynomial strain to get these constants [5]. The ability to resist deformation under pressure is measured using the bulk modulus. The ability to endure deformation increases as bulk moduli increase [6]. The resistance to shear deformation brought on by shear pressure is measured by shear modulus.

$CsGeBr_3$ in Figure 1 is perovskite structured and crystallizes in the cubic Pm3m space group. Cs^{1+} is bonded to twelve Br^{-} atoms to form $CsBr_{12}$ cuboctahedral. All Cs-Br bond lenghts are 3.91 A and Ge-Br bond lenghts are 2.77 A. $CsSiBr_3$ is a halide perovskite and has a much stronger Jahn-Teller instability than $CsGeBr_3$.

2. Methodology

The cubic structure of space group Pmm is present in the bulk perovskites of $CsGeBr_3$ and $CsSiBr_3$, and their corresponding lattice constants are 5.734 and 5.441. DFT computations were used with the Quantum Espresso programme to compare and analyse the mechanical and electrical properties [7]. The mechanical properties were examined using ultrasoft pseudopotentials for the excellent comparison with experimental data, while the valence shell and ion core electrostatic interactions of the atoms were calculated using the Generalised Gradient Approximation (GGA) of Perdew-Burke-Ernzerhof (PBE) with norm-conserving pseudopotentials treatment. In order to perform the numerical computations, we initially chose the cubic structure as a phase. The Quantum Espresso database was used to derive the pseudopotentials. In the iterative solution of the Kohn-Sham equations [8]-[14], the total energy convergence was fixed at 2×10^{-8} Ry. We fixed the plane wave energy cutoff of these systems at 550 eV, the Monkhorst-Pack scheme is utilized for the structural relaxations, and also the k-point grid is set as $12 \times 12 \times 12$. The obtained elastic constants were computed by employing the finite strain theory that was used in the Quantum espresso code. For the optimum value, the maximum strain amplitude was selected as 0.002. The convergence threshold of crystal internal stress is fixed as 0.02 Gpa. Optimised cell dimensions were fitted using the second-order Murnaghan fitting process. The kinetic energy cut-off values and the k-points were correctly optimised for convergence at the ground state energy. The Monkhost scheme [15] served as the foundation for the Brillouin sampling.

3. Results

3.1. Mechanical Properties

The two phases of $CsGeBr_3$ (cubic and tetragonal) were typically chosen as the highest temperature phases of the cubic structure to carry out the numerical computations for high-temperature device applications.

The perovskite structure is composed of corner sharing tetragonal and A-site cations in the middle of four neighbouring tetrahedra, as shown in Figure 2. The versatile perovskite structure can incorporate a large array of elements, making it possible to align its physical properties through substitutional alloying. In this perovskite, the Murnaghan Equation of State (EoS)was used to obtain the equilibrium volume, the bulk modulus and its derivatives. From thermodynamics definition, an EoS relates the volume, temperature and pressure of a material in a thermodynamic equilibrium [16] [17]. The relationship between the pressure

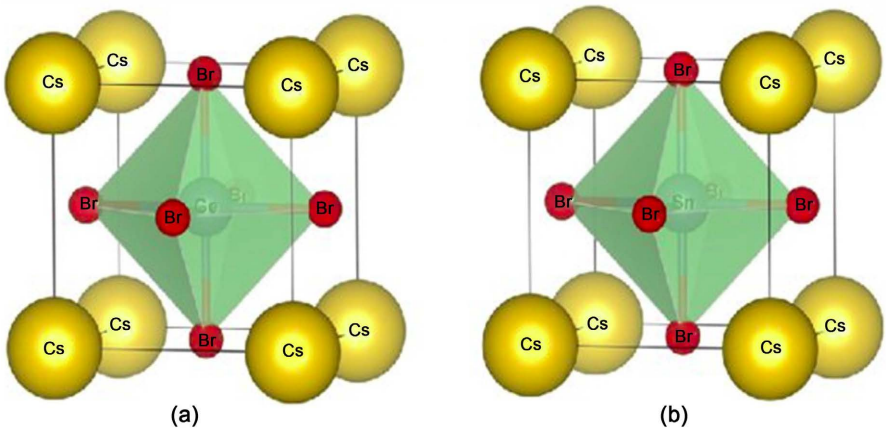

Figure 1. Cubic phase of $CsGeBr_3$ and $CsSiBr_3$ showing the position of atoms.

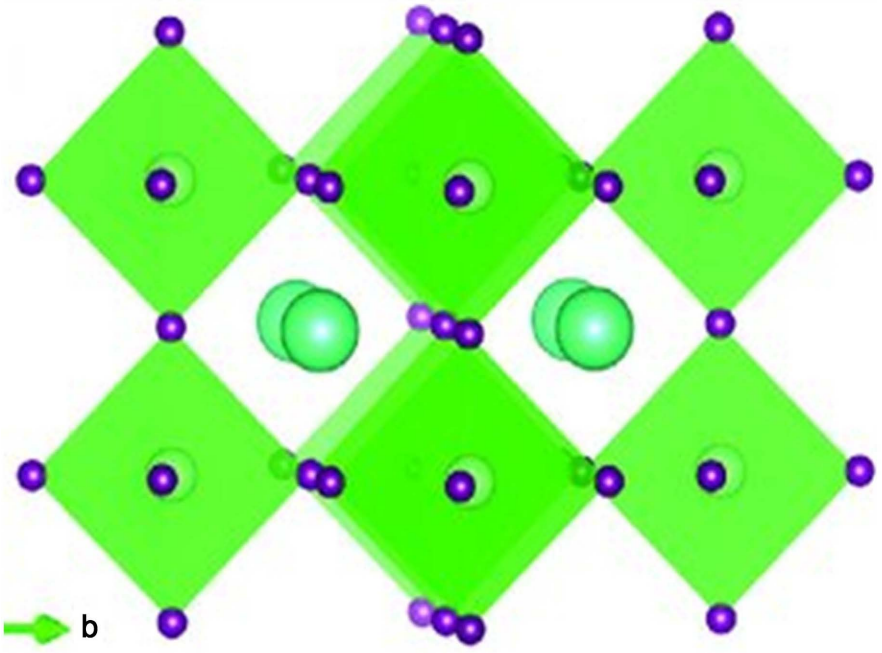

Figure 2. The perovskite structure, tetragonal Phase of $CsGeBr_3$ showing position and alignment of atoms.

and volume of a material with fixed number of particles is given by Equation (1) [17].

$$P = 1.5B_o\left[\left(\frac{v_o}{v}\right)^{\frac{7}{3}} - \left(\frac{v_o}{v}\right)^{\frac{5}{3}}\right]\left[1 + 0.75\left(B_o' - 4\right)\left(\left\{\frac{v_o}{v}\right\}^{\frac{2}{3}} - 1\right)\right] \quad (1)$$

To find the energy with respect to the volume, Equation (4.1) is integrated leading to Equation (2).

$$E(V) = E_o + \frac{9V_oB_o}{16}\left\{\left[\left(\frac{V_o}{V}\right)^{\frac{2}{3}} - 1\right]^3 B_o' + \left[\left(\frac{V_o}{V}\right)^{\frac{2}{3}} - 1\right]^2\left[6 - 4\left(\frac{V_o}{V}\right)^{\frac{2}{3}}\right]\right\} \quad (2)$$

In Quantum Espresso, the energy/volume data computed were fitted using the Murnaghan equation. This fitting was done after the lattice constant convergence was carried out from which the energies of different volumes were obtained as in Figure 3; This figure shows that the minimum energy is −2930.41 eV for $CsGeBr_3$ cubic structure showing that it is the most stable of the perovskites under study.

The volume vs energy curves are shown in Figure 3. Y1, Y2 and Y3 helps us to derive an equillibrium latice constant and the bulk modulus for the cubic and tetragonal phases of $CsGeBr_3$ and $CsSiBr_3$. The volume here is a representative of of the unit cell area. The minimum free energy for the cubic phase of CsSiBr and $CsGeBr_3$ is −2950 Ry −1900 Ry and −3200 Ry for the tetragonal phase of $CsSiBr_3$. This infers that the cubic phase is more stable than the tetragonal and monoclinic phases. This values are significant in obtaining the corresponding bulk modulus. This work used the Murnaghan (EoS) to get the equilibrium bulk modulus and its pressure derivative. It gauges a material's resistance to compression. According to [18], the volume and bulk modulus of materials are inversely connected. Equation (1) provides the bulk modulus (3).

$$B = -V\frac{\partial P}{\partial V} \tag{3}$$

where B is the bulk modulus, V the volume and P is the pressure. The pressure is given by Equation (4) below;

$$P = \frac{-\partial E}{\partial V} \tag{4}$$

Equation (4) then reduces (3) into Equation (5)

$$B = V\frac{-\partial^2 E}{\partial V^2} \tag{5}$$

The pressure derivative of the bulk modulus is given by

$$B' = \frac{\partial B}{\partial P} = \frac{1}{B}\left(V\frac{\partial}{\partial V}\left(V\frac{-\partial^2 E}{\partial V^2}\right)\right) \tag{6}$$

The relationship between pressure and volume for $CsGeBr_3$ is shown in the graph below. The position where the two lines meet indicates the minimum volume of convergence. $CsGeBr_3$ gives 1190 $(a.u)^3$ and $CsSiBr_3$ gives 1115 $(a.u)^3$ in cubic phases.

The extent of similarity is clear when pressure-volume curves in Figure 4 and Figure 5 where "pressure" is the scalar hydrostatic pressure on the periodic system. As this pressure $P = -\mathrm{d}E/\mathrm{d}V$, the optimal geometries $\mathrm{d}E/\mathrm{d}V = 0$ are now those intersecting the $P = 0$ line. The slope of one P-V curve may be used to estimate the crossing point of another hence the similarity in the P-V curvature.

Elastic properties are significant in determining the mechanical stability of compounds in solid states. The properties studied in this work are the elastic constants, the bulk modulus, Young and shear moduli and the Poisson's ratio. The elastic properties were calculated using the *thermo_pw* within Q.E. The

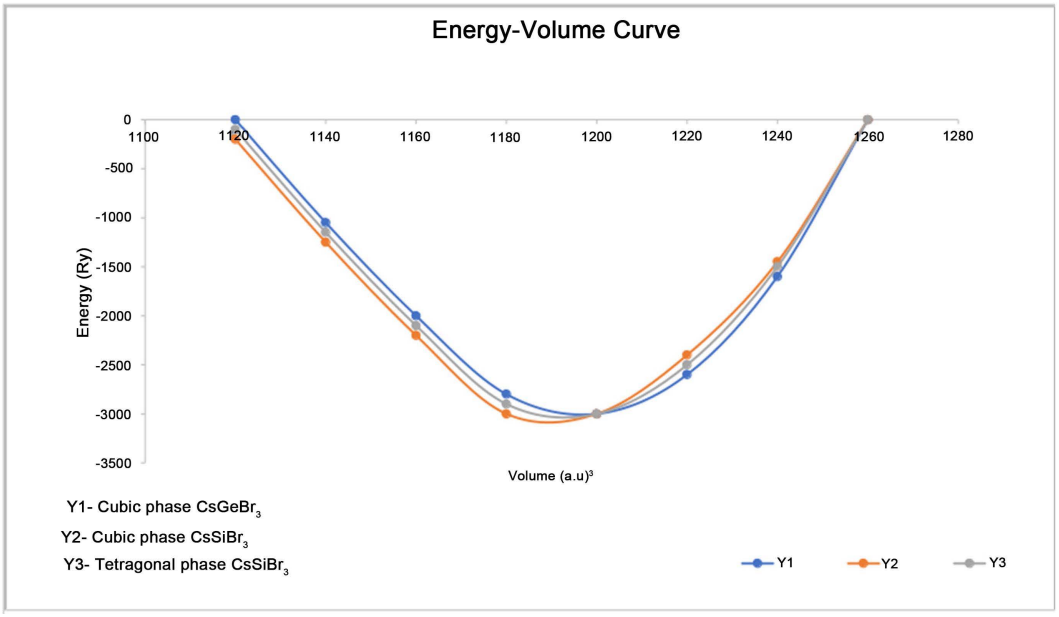

Figure 3. Energy vs Volume curve using the quantum espresso method.

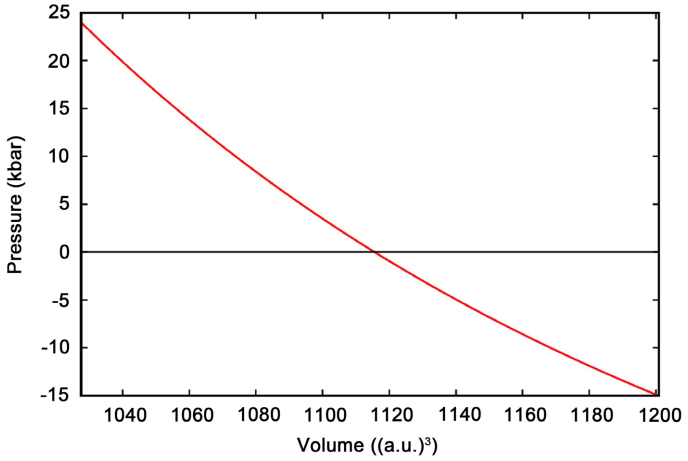

Figure 4. Pressure-volume diagram for the cubic phase of $CsGeBr_3$.

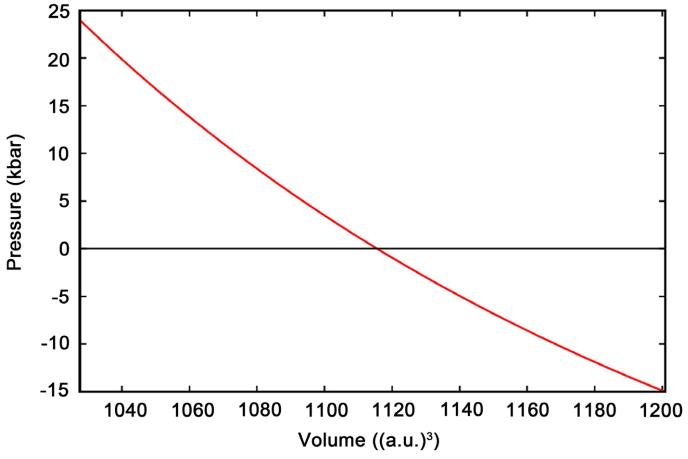

Figure 5. Pressure-volume diagram for the cubic phase of $CsSiBr_3$.

elastic constants are denoted by C_{ij} and varies from one crystal system to the other. From the Born stability criteria [19], the elastic constants need to meet certain conditions and be positive for the materials to be considered mechanically stable. In the cubic phase, the necessary conditions are given by Equations (7) [19] [20] [21] [22].

$$\begin{aligned} &C_{11}-C_{12}>0,\\ &C_{11}+2C_{12}>0,\\ &C_{44}>0 \end{aligned} \tag{7}$$

A tetragonal material is regarded mechanically stable if Equations (8) are met [19] [23];

$$\begin{aligned} &C_{11}>C_{12}\vee,\\ &2C_{13}^2<C_{33}\left(C_{11}+C_{12}\right),\\ &C_{44}>0 \end{aligned} \tag{8}$$

After the calculation of the elastic constants, the moduli are calculated using the Reuss and Voigt theory and their average obtained from the Hill averaging scheme [10]. From the C_{ij}'s, and using the Voigt theory, the bulk B_V and shear G_V moduli are given by Equations (9) and (10) respectively [23].

$$B_V=\frac{1}{9}\left[\left(C_{11}+C_{22}+C_{33}\right)+2\left(C_{12}+C_{23}+C_{31}\right)\right] \tag{9}$$

$$G_V=\frac{1}{15}\left[\left(C_{11}+C_{22}+C_{33}\right)-\left(C_{12}+C_{23}+C_{31}\right)+3\left(C_{44}+C_{55}+C_{66}\right)\right] \tag{10}$$

From the Reuss theory, the bulk B_R and shear G_R moduli are obtained from the elastic constants using Equations (11) and (12) respectively.

$$\frac{1}{B_R}=\left(S_{11}+S_{22}+S_{33}\right)+2\left(S_{12}+S_{23}+S_{31}\right) \tag{11}$$

$$\frac{15}{G_R}=4\left(S_{11}+S_{22}+S_{33}\right)-4\left(S_{12}+S_{23}+S_{31}\right)+3\left(S_{44}+S_{55}+S_{66}\right) \tag{12}$$

S_{ij}'s are the elastic compliances and are the inverse of the elastic constant's matrix. From the Hill averaging scheme, the bulk B_H and shear G_H moduli are given by the averages of the two theories, that is Equation (13) and (14) respectively.

$$B_H=\frac{B_V+B_R}{2} \tag{13}$$

$$G_H=\frac{G_V+G_R}{2} \tag{14}$$

From the Pugh method [23] brittleness or ductility of a material can be obtained by checking the relation of $\frac{B}{G}$ to the critical value of 1.75. If the ratio $\frac{B}{G}$ is more than the value, the material is considered ductile and vice versa.

After calculating the moduli and the elastic constants, the Poison's ratio and the young's modulus are obtained from the shear and bulk moduli using Equations (15) and (16) respectively [19] [20] [21] [22] [23].

$$\nu = \frac{3B_H - 2G_H}{2\left(3B_H + G_H\right)} \tag{15}$$

$$E_H = \frac{9B_H G_H}{3B_H + G_H} \tag{16}$$

The cubic and tetragonal perovskites satisfy the Born stability criterion hence they are mechanically stable [20]. The values of elastic constants for the cubic and tetragonal phases are given in **Table 1**.

The shear and moduli in the Voigt and Reuss approximations and their averages in GPa are shown in the **Table 2**. The values of B_V, G_V, B_R, G_R, B_H, G_H are obtained from Equations (9)-(14) respectively. The cubic structures had the lowest bulk moduli with the germanium compounds having low moduli than their silicon counterparts. We also noted that the monoclinic structures had inconsistent figures of both the moduli and elastic constants, showing that they are highly elastically unstable.

The Pugh criterion [5], which is employed in determining the ductile or brittle nature of materials was employed, where a material is ductile if $\frac{B}{G} > 1.75$ and brittle otherwise. From **Table 3**, the $\frac{B}{G}$ ratios obtained implies that the germanium-containing perovskites are ductile while the materials containing silicon are brittle because their $\frac{B}{G}$ ratios are less than the critical value of 1.75. The data obtained from the Poisson ratio also agree with these findings. Using the critical value of the Poisson's ratio, that is, 0.26, the materials containing germanium in the B site have $\nu > 0.26$ showing that they are ductile in nature. The perovskite materials with silicon in the B site have $\nu < 0.26$ indicating that they are brittle with the monoclinic structure having the lowest value of $0.074 < 0.26$ showing that it is highly brittle; even more than the cubic and tetragonal materials. From the calculations, the Pugh's criterion and the Poisson ratio are consistent in identifying the ductility of materials. This implies that germanium perovskite structures would crack easily especially during materials engineering for applications.

3.2. Electronic Structure Properties

Figure 6(a) depicts the band structure of $CsXBr_3$ in the BQ at ambient pressure with an FM spin configura tion in the high symmetry direction. X could be either Ge or Si. A coloured line denotes the Fermi level (EF), which is set to zero. The C-2s and Cr-3d states make up the majority of the bands in the energy range from −15 eV to −12 eV, suggesting that the Cr-3d electrons are itinerant. At practically every level, overlaps exist on top of the up- and down-spin states.

4. Discussion

This investigation focused on the mechanical and electrical structural characteristics of perovskite-type $CsXBr_3$ (X = Ge or Si) compounds in the cubic and

Table 1. The calculated elastic constants (C_{ij}) measured in GPa.

Material	C_{11}	C_{12}	C_{13}	C_{33}	C_{44}	C_{55}	C_{66}
Ge Cubic	46.866	10.184			9.624		
Si Cubic	47.726	12.325			12.126		
Ge Tetragonal	41.246	21.301	10.486	38.908	9.372		9.372
Si Tetragonal	44.894	19.376	11.813	39.597	11.683		11.683

Table 2. The bulk (B_V, B_R, B_H) and shear (G_V, G_R, G_H) moduli.

Material	B_V	B_R	B_H	G_V	G_R	G_H
Ge Cubic	22.411	22.411	22.411	13.111	11.883	12.497
Si Cubic	24.126	24.126	24.126	14.356	13.874	14.115
Ge Tetragonal	22.883	22.720	22.802	13.002	11.755	12.378
Si Tetragonal	23.932	23.800	23.866	14.237	13.700	13.969

Table 3. The Poisson's ratio (ν, Young's modulus E_H in GPa, Cauchy pressure and the $\frac{B}{G}$.

Material	$\frac{B}{G}$	ν	E_H
Ge Cubic	1.793	0.264	31.604
Si Cubic	1.709	0.255	35.433
Ge Tetragonal	1.842	0.270	31.436
Si Tetragonal	1.708	0.255	35.063

tetragonal phases. The materials demonstrate that they are elastically stable since the elastic constant values obtained are in agreement with the four Born and Huang criteria. $CsGeBr_3$ is found to have the highest bulk modulus value, whilst $CsSiBr_3$ has the lowest value. According to the conclusions drawn, $CsGeBr_3$'s cubic and tetragonal phases are stiffer than the monoclinic phases and compounds. Despite the fact that $CsGeBr_3$ has a larger Poisson's ratio than $CsSiBr_3$,it may be inferred that both substances are brittle. The energy range between 7.0 and 5.0 eV corresponds to the effective energy that is related to these materials' primary electronic characteristics. In the unit cell of these compounds, some atoms with several orbitals combine to generate the sub-bands.

5. Conclusion

The application of these materials in solar cell devices is compared by the aforementioned property and phase investigation. For a suitable solar cell application, we estimated the mechanical and electrical responses of the two phases of $CsGeBr_3$ and $CsSiBr_3$. The experimental data showed excellent agreement with the optimised lattice constant and elastic constant. Theoretically, it was discovered

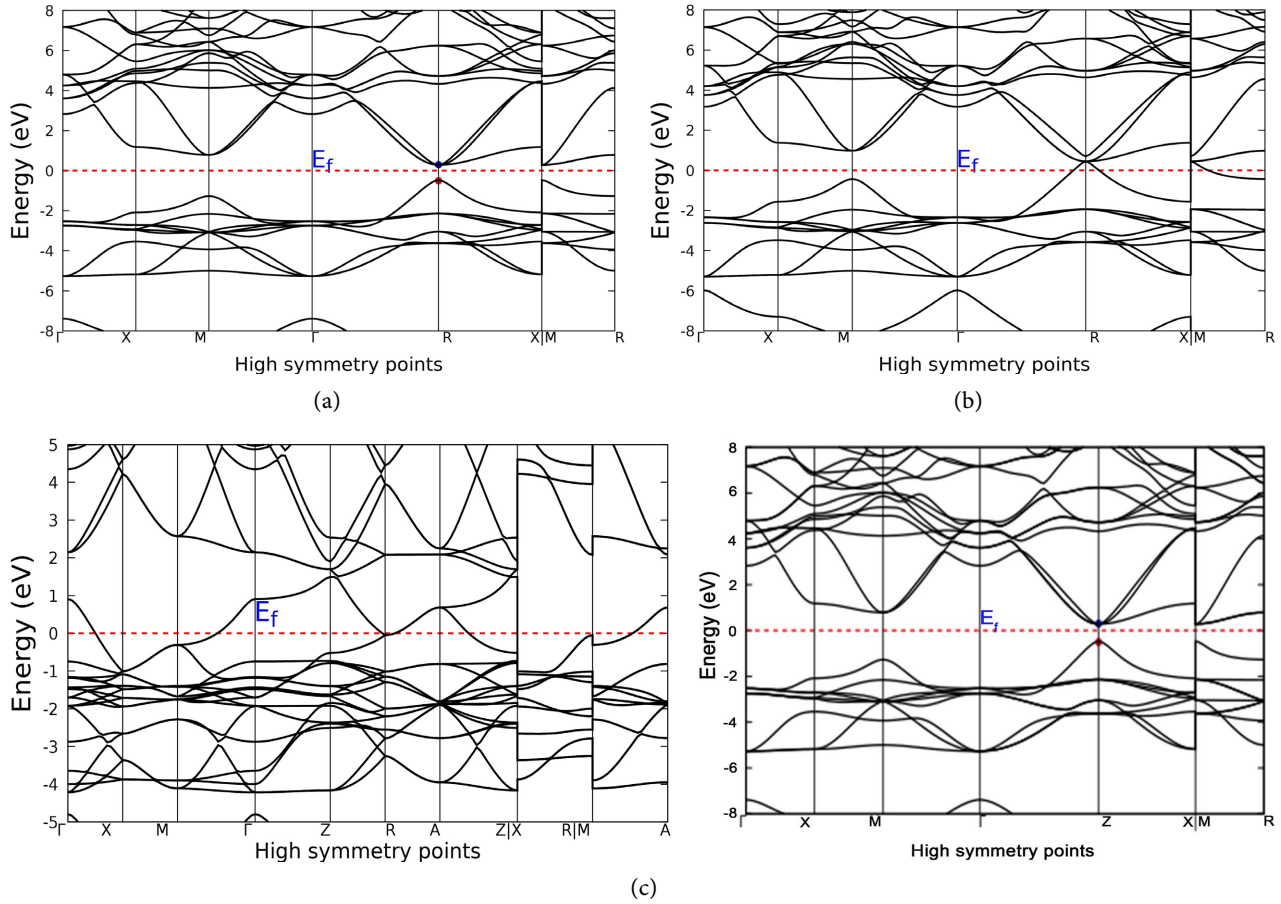

Figure 6. (a) Band structure for $CsGeBr_3$ Cubic Phase; (b) Band structures for $CsSiBr_3$ Cubic Phase; (c) Band structures for $CsGeBr_3$ and $CsSiBr_3$ tetragonal phases.

that $CsGeBr_3$ has the most stable oxidation, making it the most stable photocatalyst. $CsXBr_3$ (X = Ge and Si) compounds' electrical and optical characteristics were calculated using first-principles calculations.

Acknowledgements

The computational tools necessary for this work's success were supplied by the Centre for High Performance Computing (CHPC), South Africa, and the authors are grateful for their support.

Conflicts of Interest

The authors declare no conflicts of interest regarding the publication of this paper.

References

[1] Wang, J., Fu, X.N., Zhang, X.D. and Jiang, Z.Y. (2016) The Frontiers of Physics.

[2] Ren, M., Qian, X.F., Chen, Y.T., Wang, T.F. and Zhao, Y.X. (2022) Potential Lead Toxicity and Leakage Issues on Lead Halide Perovskite Photovoltaics. *Journal of Hazardous Materials*, **426**, Article ID: 127848.

[3] Shi, Z.Q. and Jayatissa, A.H. (2018) Perovskite—Based Solar Cell: A Review of Recent Progress, Materials and Processing Methods. *Materials* (*Basel*), **11**, Article 729. https://vdoc.pub/documents/kelvin-probe-force-microscopy-7t6pifs21eb0

[4] Jong, U.G., Yu, C.J., Kye, Y.H., Choe, Y.G., Hao, W. and Li, S. (2019) First-Principles Study on Structural, Electronic, and Optical Properties of Inorganic Ge-Based Halide Perovskites. *Inorganic Chemistry*, **58**, 4134-4140. https://pubmed.ncbi.nlm.nih.gov/30864433/ https://doi.org/10.1021/acs.inorgchem.8b03095

[5] Pugh, S.F. (1954) Relations between the Elastic Moduli and the Plastic Properties of Polycrystalline Metals. *Journal of Science*, **45**, 823-843. https://doi.org/10.1080/14786440808520496

[6] Cherkaev, A. and Gibiansky, H. (1993) Coupled Estimates for the Bulk and Shear Moduli of a Two-Dimensional Isotropic Elastic Composite. *Journal of the Mechanics and Physics of Solids*, **41**, 937-980. https://www.sciencedirect.com/science/article/pii/0022509693900062 https://doi.org/10.1016/0022-5096(93)90006-2

[7] Giannozzi, P., *et al.* (2009) QUANTUM ESPRESSO: A Modular and Open-Source Software Project for Quantum Simulations of Materials. *Journal of Physics*: *Condensed Matter*, **21**, Article ID: 395502. https://doi.org/10.1088/0953-8984/21/39/395502

[8] Singh, D.J. and Du, M.H. (2008) Density Functional Study of LaFeAsO(1-x)F(x): A Low Carrier Density Superconductor Near Itinerant Magnetism. *Physical Review Letters*, **100**, Article ID: 237003. https://pubmed.ncbi.nlm.nih.gov/18643537/

[9] Dias, A.C., Lima, M.P. and Da Silva, J.L.F. (2021) Role of Structural Phases and Octahedra Distortions in the Optoelectronic and Excitonic Properties of $CsGeX_3$ (X = Cl, Br, I) Perovskites. *The Journal of Physical Chemistry C*, **125**, 19142-19155. https://doi.org/10.1021/acs.jpcc.1c05245

[10] Hill, R. and Milstein, F. (1977) Principles of Stability Analysis of Ideal Crystals. *Physical Review B*, **15**, 3087-3096. https://journals.aps.org/prb/abstract/10.1103/PhysRevB.15.3087 https://doi.org/10.1103/PhysRevB.15.3087

[11] Hill, R. (1952) Elastic Behaviour of a Crystalline Aggregate. *Proceedings of the Physical Society*: *Section A*, **65**, 349-354. https://iopscience.iop.org/article/10.1088/0370-1298/65/5/307 https://doi.org/10.1088/0370-1298/65/5/307

[12] Lin, L., *et al.* (2013) Efficient Iterative Method for Solving the Dirac-Kohn-Sham Density Functional Theory. https://math.berkeley.edu/~linlin/publications/RelDFT.pdf

[13] Giannozzi, P., *et al.* (2009) Quantum Espresso: A Modular and Open-Source Software Project for Quantum Simulations of Materials. *Journal of Physics: Condensed Matter*, **21**, Article ID: 395502. https://doi.org/10.1088/0953-8984/21/39/395502

[14] Kohn, W. and Sham, L.J. (1965) Self-Consistency Equations Including and Correlation Exchange Effects. *Physical Review Journals Archive*, **140**, A1133-A1138. https://doi.org/10.1103/PhysRev.140.A1133

[15] Monkhorst, H.J. and Pack, J.D. (1976) Special Points for Brillouin-Zone Integrations. *Physical Review B*, **13**, 5188-5192. https://journals.aps.org/prb/abstract/10.1103/PhysRevB.13.5188 https://doi.org/10.1103/PhysRevB.13.5188

[16] Mansour, S.F., Al-Wafi, R. and Abdo, M.A. (2016) Zn-Mg-La Nanoferrites for Sto-

rage and High Frequency Devices with Augmenting the Photocatalytic Performance. *Journal of Alloys and Compounds*, **826**, Article ID: 154125. https://doi.org/10.1016/j.jallcom.2020.154125

[17] Tyuterev, V.G. and Vast, N. (2006) Murnarghan's Equation of State for Electronic Ground State Energy. *Computation Material Science*, **38**, 350-353. https://www.researchgate.net/publication/229264555

[18] Zahrouni, A., Benammar, I., Harzallah, O. and Bistac, S. (2023) Mechanical and Thermal Properties of a Nanocomposite Made of Polymer Matrix reinforced by a Binary Nanoparticle TiO_2-SiO_2 Produced by Sol-Gel Method. https://www.researchgate.net/publication/368515750

[19] Mouhat, F. and Coudert, F.X. (2014) Necessary and Sufficient Elastic Stability Conditions in Various Crystal Systems. *Physical Review B*, **90**, Article ID: 224104. https://arxiv.org/pdf/1410.0065.pdf https://doi.org/10.1103/PhysRevB.90.224104

[20] Zhang, J.M., Zhang, Y., Xu, K.W. and Ji, V. (2007) Young's Modulus Surface and Poisson's Ratio Curve for Cubic Metals. *Journal of Physics and Chemistry of Solids*, **68**, 503-510. https://www.researchgate.net/publication/264672862 https://doi.org/10.1016/j.jpcs.2007.01.025

[21] Li, H., Fan, C. and Lou, W. (2017) Necessary and Sufficient Elastic Stability Conditions in 21 Quasicrystal Laue Classes. *European Journal of Mechanics*, **65**, 30-39. https://arxiv.org/pdf/1410.0065.pdf https://doi.org/10.1016/j.euromechsol.2017.02.007

[22] Hou, Z.F. (2008) *Ab initio* Calculations of Elastic Modulus and Electronic Structures of Cubic $CaZrO_3$. *Physica B*: *Condensed Matter*, **403**, 2624-2628. https://doi.org/10.1016/j.physb.2008.01.025

[23] Dong, Y.L., Wu, X.W. and Martini, A. (2013) Atomic Roughness Enhanced Friction on Hydrogenated Graphene. *Nanotechnology*, **24**, Article ID: 375701. https://iopscience.iop.org/article/10.1088/0957-4484/24/37/375701/meta https://doi.org/10.1088/0957-4484/24/37/375701